

Cite this article as: Nie Kaibo, Yang An, Deng Kunkun, et al. Effect of Extrusion Parameters on Microstructure and Mechanical Properties of SiC Particle Reinforced Mg-3.6Zn-0.6Y-0.2Ca Matrix Composites[J]. Rare Metal Materials and Engineering, 2021, 50(04): 1187-1195.

Effect of Extrusion Parameters on Microstructure and Mechanical Properties of SiC Particle Reinforced Mg-3.6Zn-0.6Y-0.2Ca Matrix Composites

Nie Kaibo^{1,2}, Yang An², Deng Kunkun^{1,2}, Kang Xinkai¹, Li Yanan¹

¹ College of Materials Science and Engineering, Taiyuan University of Technology, Taiyuan 030024, China; ² Shanxi Key Laboratory of Advanced Magnesium-Based Materials, Taiyuan University of Technology, Taiyuan 030024, China

Abstract: The microstructures and mechanical properties of a newly developed Mg-3.6Zn-0.6Y-0.2Ca matrix composite containing SiC particle before and after extrusion were investigated. Results show that the grain sizes of the as-extruded composites decrease as compared to the as-homogenized composite before extrusion. With increasing the extrusion speed or extrusion temperature, the size of recrystallized grains increases while the volume fraction slightly increases. The size of dynamic precipitated phases increases and the volume fraction decreases with increasing the extrusion speed. With an increase in extrusion speed from 0.01 mm/s to 0.1 mm/s at 230 °C or extrusion temperature from 190 °C to 230 °C at 0.1 mm/s, the yield strength and ultimate tensile strength decrease while the elongation increases. The yield strength, ultimate tensile strength and elongation of composites extruded under optimized extrusion parameters (190 °C, 0.1 mm/s) are 312.0 MPa, 347.3 MPa and 6.6%, respectively. The contribution of grain refinement strengthening to the strength increment is higher relative to the thermal expansion effect and precipitate strengthening.

Key words: SiC_p/Mg-Zn-Y-Ca composite; hot extrusion; microstructure; mechanical properties

Magnesium alloys with high specific strength, low density and high energy absorption, have attracted great attention as promising candidates in lightweight structural transportation sector which demands for energy saving and reduction of gas emission^[1]. However, magnesium alloys usually provide inadequate strength of yield strength much lower than ~300 MPa^[2,3], which seriously hinders their widespread applications. To develop an industry-acceptable magnesium alloy, tremendous attempts have been made in the introduction of various alloying elements to improve comprehensive properties^[4]. Considering the difference in solid solubility of alloying elements, large quantity of Zn or rare earth (RE) elements have been commonly used due to their strong precipitation and grain boundary strengthening^[5,6]. For instance, Xu et al developed a wrought Mg-Gd-Y-Zn-Zr alloy, which exhibited an ultra-high-strength over 500 MPa after deformation and aging^[7]. However, the addition of high concentration of heavy RE or Zn elements inevitably leads to an obvious increase in the den-

sity and material cost, as well as a decrease in formability and poor weldability. In this situation, trace elements including La, Ce, Zr, Mn, Gd and Y have been added singly, doubly and even multiply^[8-10]. Especially, low Zn-containing magnesium alloys have been developed by the combined addition of RE elements and other non-RE elements, which possess high ductility and excellent formability^[9-10]. Further, it has been reported that minor addition of specific elements such as calcium (Ca) can improve the flame-retardant property of magnesium alloy, which is beneficial to the melting of magnesium alloys^[11]. Thus, a Mg-3.6Zn-0.6Y-0.2Ca alloy, with minor addition of Ca and Y developed in our previous work^[12], was selected as matrix alloy in the present work.

Besides the alloying element addition, the preparation of magnesium matrix composites by adding various reinforcements (such as SiC, B₄C, TiC and Al₂O₃) can also significantly improve the performance of the magnesium alloy^[13-16]. Wu et al^[17] reported that AZ91 matrix composite containing SiC par-

Received date: April 18, 2020

Foundation item: National Natural Science Foundation of China (51771129, 51401144, 51771128)

Corresponding author: Nie Kaibo, Ph. D., Professor, College of Materials Science and Engineering, Taiyuan University of Technology, Taiyuan 030024, P. R. China, Tel: 0086-351-6010021, E-mail: niekaibo@tyut.edu.cn

Copyright © 2021, Northwest Institute for Nonferrous Metal Research. Published by Science Press. All rights reserved.

ticles exhibit a higher yield strength relative to unreinforced AZ91 alloy, while the elongation decreases. In addition, the previous researches have shown that micro-sized particles can stimulate recrystallization, contributing to the grain boundary strengthening and load transfer^[18]. However, the high content of particulate reinforcements can inevitably deteriorate the ductility of magnesium matrix composite in addition to significantly improving the specific modulus and strength. Therefore, a suitable concentration of micro-sized ceramic particles should be applied to increase strength with little negative impact on the ductility. Further, the microstructure and properties of magnesium matrix composite can be optimized by conventional secondary processing, especially hot extrusion^[19]. Li et al reported that a Mg-4Zn-0.5Ca matrix composite containing 2vol% micro-sized SiC particles possessed a simultaneous improvement in yield strength, ultimate tensile strength and ductility after hot extrusion as compared to the unreinforced Mg-4Zn-0.5Ca alloy^[20]. Thus, a combination of high strength and comparable ductility is expected to achieve for the magnesium matrix composites through the addition of low content of external ceramic particles. Based on extensive literature searches, there are few studies reported on the exact effect of extrusion parameters on a low-alloying Mg-Zn-Y-Ca magnesium alloy containing low concentration of micro-sized particles.

Accordingly, in this study, a new low-alloying Mg-3.6Zn-0.6Y-0.2Ca matrix composite reinforced by 2vol% SiC particles was prepared and then extruded. Systematic investigation was conducted on the effects of extrusion parameters (extrusion temperature and speed) on microstructure, texture and mechanical properties of the SiC_p/Mg-3.6Zn-0.6Y-0.2Ca composites.

1 Experiment

In this study, SiC particles with a diameter size of 5 μm and volume fraction of 2vol% were selected as reinforcing particles. A low alloyed Mg-3.6Zn-0.6Y-0.2Ca (wt%) was used as matrix alloy. Firstly, commercially pure Mg (99.99wt%), Zn (99.99wt%), Ca (99.99wt%) and Mg-30wt%Y master alloy were melt at 720 °C in an electrical resistance furnace in a mild steel crucible coated with boron nitride under a cover gas mixture of CO₂ and SF₆. Second, the temperature of melt was reduced to 600 °C, and the SiC particles (preheated to 600 °C) were introduced by semi-solid stirring. The composite melt after stirring for 20 min was raised to 720 °C and poured into the mold (preheated to 250 °C).

Before extrusion, the as-cast composites with a diameter of 40 mm were homogenized (400 °C/8 h). The extrusion temperatures were set as 230 and 190 °C at a constant extrusion speed of 0.1 mm s⁻¹ while the extrusion speeds were determined as 0.01 and 0.1 mm s⁻¹ at 230 °C. The sample for extrusion was heated to preset extrusion temperature and extruded at a fixed extrusion ratio of 16:1.

The microstructure observation for the SiC_p/Mg-3.6Zn-0.6Y-0.2Ca composite was performed on an optical microscopy (OM), scanning electron microscopy (SEM) equipped with energy dispersive spectrometer (EDS). The specimens for OM

and SEM cut along the extrusion direction were prepared by a standard procedure involving the grinding, polishing and etching using an oxalic solution (4 g oxalic acid+100 mL deionized water). Thin films processed by the combination of mechanical thinning and ion-beam milling techniques were used for transmission electron microscopy (TEM). The phase compositions were identified by X-ray diffraction (XRD). The statistics of volume fractions and average sizes were realized for both the dynamic recrystallized (DRXed) grains and second phases using Image-Pro Plus (IPP) software. The volume fractions of DRXed grains (V_{DRX}) for the as-extruded composites were defined as follows^[20]: $V_{\text{DRX}} = S_{\text{DRX}} / (S_{\text{DRX}} + S_{\text{unDRX}})$, where S_{DRX} and S_{unDRX} stand for the area of DRXed and unDRXed regions, respectively. The texture examinations of the extruded composites were carried out by a Rigaku D/max-2400 X-ray diffractometer. The pole figures were obtained and the texture data were analyzed using PANalytical X'Pert Texture.

The rods were machined into tensile specimen with a gauge length of 54 mm and cross-sectional areas of 6 mm×2 mm. The tensile tests with tensile directions parallel to the extrusion direction were performed on an Instron Series 3369 test machine at the tensile rate of 0.5 mm/min at room temperature. A total of three tensile specimens for each sample were measured to verify the reproducibility.

2 Results and Discussion

2.1 Microstructures of SiC_p/Mg-3.6Zn-0.6Y-0.2Ca composite

The OM images and secondary electron micrographs of SiC_p/Mg-3.6Zn-0.6Y-0.2Ca composites before extrusion are shown in Fig. 1. As can be seen in Fig. 1a, the grain size of as-homogenized composite is coarse, with many black phases distributed along the grain boundaries. At higher magnification in Fig. 1b, some particulate phases can be clearly observed. As shown in Fig. 1c, the distribution of the particulate phases is relatively uniform in the matrix, and the compositions can be determined as SiC particles according to the results of EDS analysis as given in Fig. 1d. The added SiC particles can be pushed by the solid-liquid interface during the solidification of composite^[21], resulting in the distribution along the grain boundaries in the present work. Further, it is reported that the as-homogenized Mg-3.6Zn-0.6Y-0.2Ca alloy without SiC particles is composed of *α*-Mg and a thermally stable icosahedral quasicrystal phase (I-phase)^[12,22]. Thus, the fine plate-like phases in the Mg-3.6Zn-0.6Y-0.2Ca matrix composite should be also I-phases since the addition of ceramic SiC particles does not change the phase composition.

Optical micrographs of SiC_p/Mg-3.6Zn-0.6Y-0.2Ca composites processed under different extrusion parameters are shown in Fig. 2. It is obvious that due to the occurrence of dynamic recrystallization (DRX), the grains are significantly refined after extrusion as compared to the as-homogenized counterpart. The distribution of SiC particles and second phases is changed into strip along the extrusion direction (ED). It can be clearly seen that there are still some unDRX regions for the

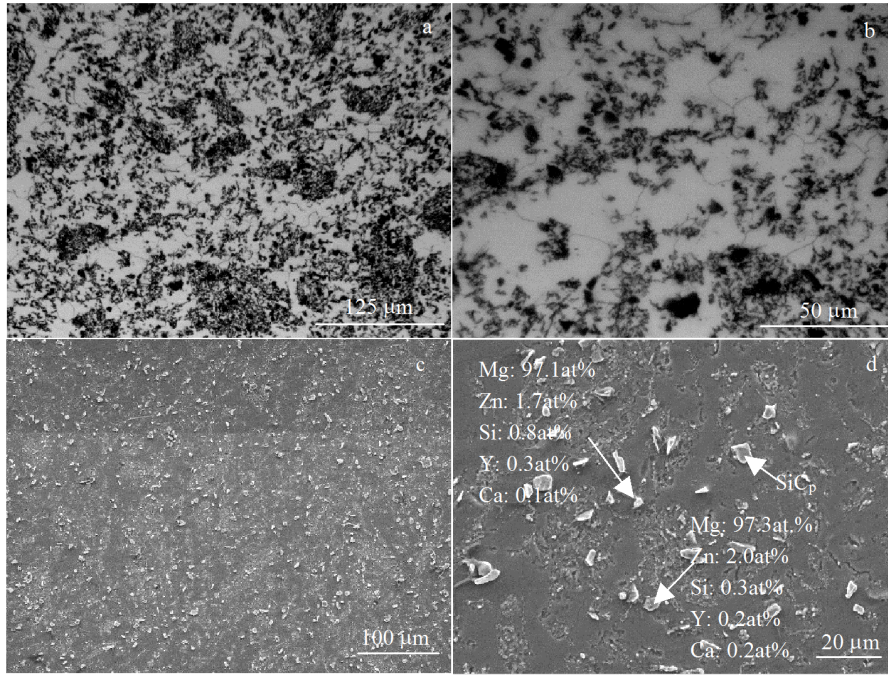


Fig.1 OM (a, b) images; SEM images and EDS analysis (c, d) of $\text{SiC}_p/\text{Mg-3.6Zn-0.6Y-0.2Ca}$ composites before extrusion

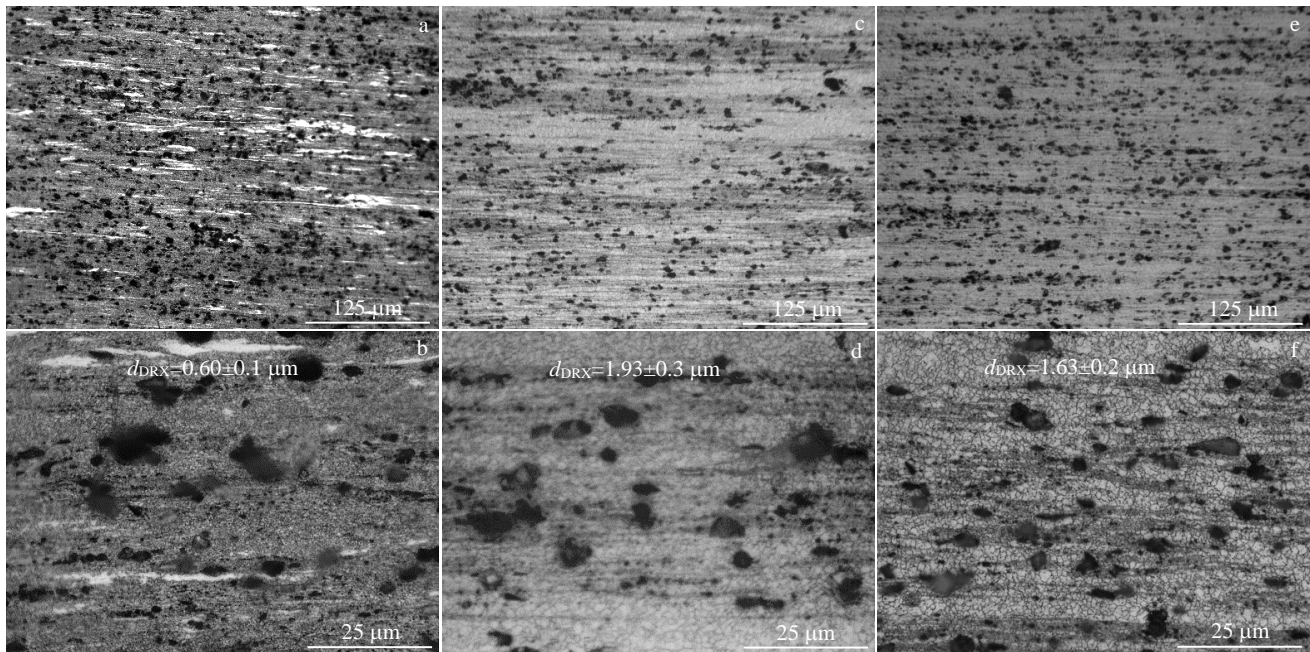


Fig.2 OM images of $\text{SiC}_p/\text{Mg-3.6Zn-0.6Y-0.2Ca}$ alloys extruded under different extrusion parameters (d_{DRX} -average size of DRX): (a, b) 0.1 mm/s, 190 °C; (c, d) 0.1 mm/s, 230 °C; (e, f) 0.01 mm/s, 230 °C

composite extruded at 190 °C. As the extrusion temperature increases to 230 °C, the unDRX region gradually disappears and the DRX tends to be complete. By comparing it to the composite extruded at 190 °C (Fig.2a and 2c), the increase in extrusion temperature leads to a larger grain size. As the extrusion speed reduces from 0.1 $\text{mm}\cdot\text{s}^{-1}$ to 0.01 $\text{mm}\cdot\text{s}^{-1}$ at 230 °C, the average grain size

of the composites decrease from 1.93 μm to 1.63 μm .

Fig.3 shows the XRD patterns of $\text{SiC}_p/\text{Mg-3.6Zn-0.6Y-0.2Ca}$ composites extruded at 230 °C. The as-extruded composites are comprised of five phases including α -Mg, I phase, SiC, $\text{Ca}_2\text{Mg}_6\text{Zn}_3$, and MgZn_2 phases, as shown in Fig.3. Since the composite has been homogenized before extrusion, there

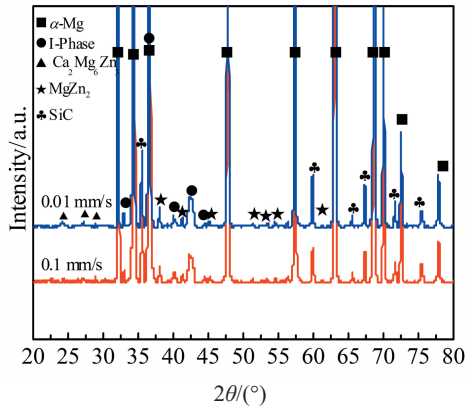


Fig.3 XRD patterns of SiC_p/Mg-3.6Zn-0.6Y-0.2Ca composites extruded at 230 °C and different extrusion speeds

should be dynamic precipitation of the MgZn₂ phase and I phase during extrusion. SEM was used to further analyze the second phases in the SiC_p/Mg-3.6Zn-0.6Y-0.2Ca composites, as shown in Fig.4. Fine dynamic precipitates are uniformly dispersed within the grains and at the grain boundaries after extrusion (Fig.4a~4c). According to the EDS results (Table 1), the precipitated phases are mainly composed of Mg, Zn and a small amount of Y elements. According to the XRD patterns shown in Fig.3, these precipitated phases are determined as I phase or MgZn₂.

The statistical results of average sizes and volume fractions for the precipitated phases are given in Fig.5. The precipitated phases tend to grow up with raising the extrusion temperature, while their volume fractions increase. As the extrusion speed decreases from 0.1 to 0.01 mm·s⁻¹, the volume fraction of precipitates increases while the average size decreases. Fig.6 shows the TEM image and EDS spectra of SiC_p/Mg-3.6Zn-0.6Y-0.2Ca composites after extrusion at 230 °C. As shown in Fig.6, the grain boundaries of DRXed grains are very flat and equiaxed, indicating that the DRX process is almost complete. According to the EDS spectrum of precipitated phases marked by the arrow in Fig.6a, the main elements are Mg and Zn, and in combination with the XRD results in Fig.3, it can further confirm the dynamic precipitation of MgZn₂,

phase in the present SiC_p/Mg-3.6Zn-0.6Y-0.2Ca composite.

In general, the grain sizes and volume fractions of as-extruded magnesium-based materials are influenced by both the grain sizes before extrusion and extrusion parameters. For the present SiC_p/Mg-3.6Zn-0.6Y-0.2Ca composites, the effect of extrusion temperature and strain rate on the average grain sizes can be described by the Zener-Hollomon parameters (Z)^[23]:

$$Z = \dot{\epsilon} \exp(Q/RT) \quad (1)$$

where $\dot{\epsilon}$, Q , R and T are the strain rate, activation energy, gas constant and deformation temperature, respectively. The recrystallized grain size (d_{DRX}) is related to Z value, which can be expressed as^[24]:

$$Zd_{\text{DRX}}^m = A \quad (2)$$

where m represents the power law exponent and A is a constant. According to Eq.(2), the grain size decreases as the value of Z increases. With a decrease in extrusion temperature from 230 °C to 190 °C, the Z value increases and thus DRXed grain size decreases. An increase in the extrusion speed leads to a reduction in heat dissipation, so the actual extrusion temperature experienced by the sample increases^[25], which contributes to the grain growth. Further, the size of DRXed grains can be affected by the size and the distribution of particulate phases. On the one hand, the added large-sized SiC particles larger than 1 μm were hardly plastically deformed during extrusion^[18], which can lead to the formation of particle deformation zone (PDZ) around SiC particles. The PDZ with high-density dislocations and large orientation difference gradient can promote the occurrence of DRX during extrusion, resulting in the nearly full recrystallization of the SiC_p/Mg-3.6Zn-0.6Y-0.2Ca composite. On the other hand, the fine precipitates less than 1 μm can inhibit the growth of DRXed grains through Zener pinning effect^[15]. The volume fraction of precipitates significantly decreases with increasing the extrusion speed from 0.01 mm/s to 0.1 mm/s for the present composite (Fig.5), resulting in the weakening of pinning effect on the grain boundaries, and thus leading to the increase in grain size. Further, the volume fraction of DRXed grains for the present composite is significantly increased relative to the unreinforced alloy^[12], indicating that the addition of SiC_p can effectively promote the occurrence of DRX.

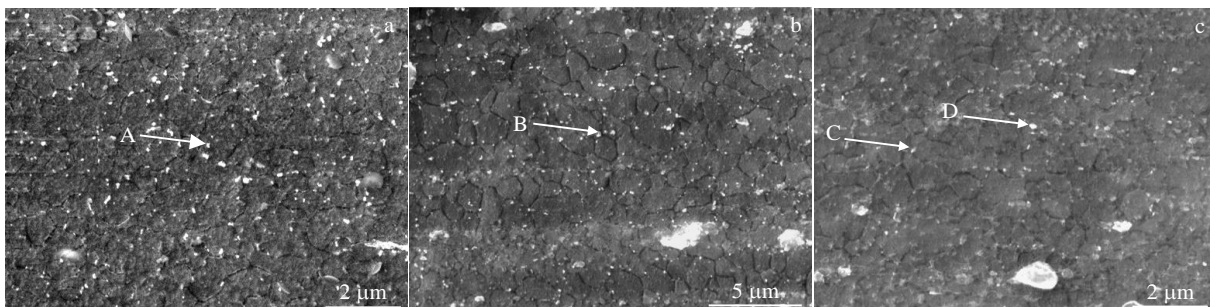
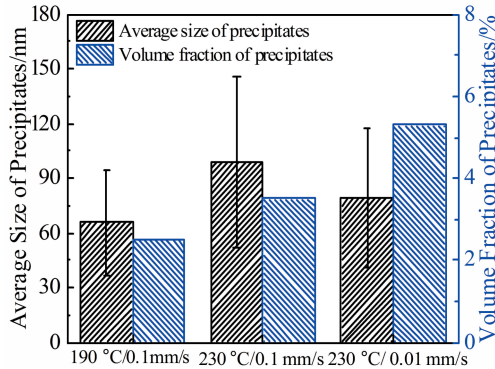
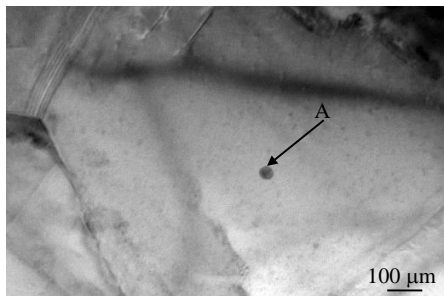


Fig.4 SEM images of SiC_p/Mg-3.6Zn-0.6Y-0.2Ca composites extruded under different extrusion parameters: (a) 0.1 mm/s, 190 °C; (b) 0.1 mm/s, 230 °C; (c) 0.01 mm/s, 230 °C

Table 1 EDS results of arrow positions of SiC_p/Mg-3.6Zn-0.6Y-0.2Ca composites extruded under different conditions in Fig.4

Position	Element content/at%				Possible phase
	Mg	Zn	Y	Si	
A	98.0	1.6	0.1	0.3	I Phase (Mg ₃ Zn ₆ Y)
B	98.1	1.6	0	0.2	
C	98.3	1.5	0.1	0	
D	95.8	3.6	0	0.5	

Fig.5 Statistical results of average size and volume fraction of the precipitates in SiC_p/Mg-3.6Zn-0.6Y-0.2Ca composites

Point A	wt%	at%
Mg K	78.59	90.80
Zn K	21.41	9.20

Fig.6 TEM and EDS results of SiC_p/Mg-3.6Zn-0.6Y-0.2Ca composites extruded at 230 °C/0.1 mm·s⁻¹

With regarding to the precipitation of secondary phases during the DRX, it is controlled by two processes of nucleation and growth. The faster the extrusion speed, the greater the heat of extrusion, resulting in an increase in actual temperature experienced by the extrusion sample. As described by Fick's first law of the diffusion^[26]:

$$D = D_0 \exp(-Q/RT) \quad (3)$$

where D , D_0 , Q and T represent the diffusion coefficient, diffusion constant, activation energy and temperature, respectively. The actual temperature experienced for the sample extruded at

230 °C/0.1 mm·s⁻¹ is higher than that of sample extruded at 230 °C/0.01 mm·s⁻¹, which is conducive to the growth of newly formed nano-sized precipitates. Further, previous studies have shown that the faster the extrusion speed, the higher the rate for the vacancy formation^[21], and the easier it is for vacancies to aggregate, which facilitates the diffusion of Zn and Y atoms. The size of precipitated phases increases with increasing the extrusion speed due to the combination of the above factors. At the same time, there are many crystal defects such as vacancies and dislocations in the grain boundaries, which can serve as the preferential nucleation sites^[26]. The higher the DRX grain sizes, the smaller the total areas for the grain boundaries, so the number of potential nucleation sites decreases with increasing the extrusion speed, leading to a reduction in the number of the precipitated phases. Thus, as the extrusion speed increases, the size of the precipitated phase increases and the volume fraction decreases. As the extrusion temperature increases, the atomic diffusion rate increases, and the growth of the precipitation phase is more pronounced, which leads to an increase in the size. However, as the extrusion temperature increases, the total grain boundary area decreases, which can decrease the nucleation rate, decreasing the volume fraction of the precipitated phases.

Fig.7 shows the XRD macrottextures of SiC_p/Mg-3.6Zn-0.6Y-0.2Ca composites extruded under different conditions. It can be seen from Fig.7 that all the composites exhibit a (0002) basal texture. The texture intensity is mainly related to the volume fraction of unDRXed grains and dynamically precipitated phases^[12]. Further, the previous studies have shown that the growth of recrystallized grains can also increase the texture intensity^[9]. By comparing Fig.7a with 7c, the texture intensity extruded at 0.01 mm/s is significantly lower than that at 0.1 mm/s at the same extrusion temperature of 230 °C. The DRX volume fraction after extrusion at 0.01 mm/s is slightly lower while DRXed grain size is finer relative to that extruded at 0.1 mm/s. Furthermore, the volume fraction of the precipitated phases is higher in the sample extruded at 0.01 mm/s, which can produce a stronger pinning effect on the DRX grains during the extrusion. These combined effects lead to lower basal texture intensity after extrusion at 0.01 mm/s. With an increase in extrusion temperature from 190 °C to 230 °C, as shown in Fig.7b and 7c, the texture intensity of (0002) pole figures increases. This can be ascribed to the larger DRXed grain sizes, which possess a certain preferred orientation. In addition, <11 $\bar{2}$ 0> fiber textures can be observed in the inverse pole figures of the composites. However, the <11 $\bar{2}$ 0> direction in the inverse pole figure extruded at 230 °C/0.1 mm s⁻¹ rotates to <11 $\bar{2}$ 0> rare earth texture direction, which may be ascribed to the coarser DRXed grain size. This phenomenon is consistent with the appearance of RE texture components only found in microstructure of large DRXed grain reported by Stanford et al^[27].

2.2 Mechanical properties of SiC_p/Mg-3.6Zn-0.6Y-0.2Ca composite

Fig.8a shows the curves of engineering stress versus engineering strain for the SiC_p/Mg-3.6Zn-0.6Y-0.2Ca composites

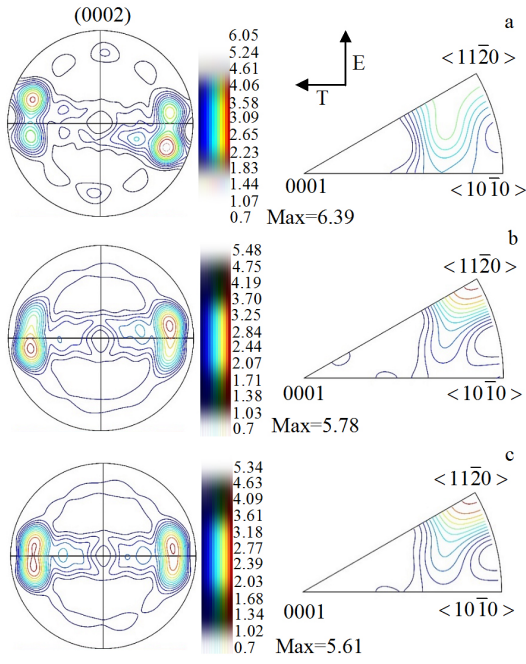


Fig.7 (0002) pole figures and inverse pole figures of SiC_p/Mg-3.6Zn-0.6Y-0.2Ca composites under different extrusion parameters: (a) 0.1 mm/s, 190 °C; (b) 0.1 mm/s, 230 °C; (c) 0.01 mm/s, 230 °C

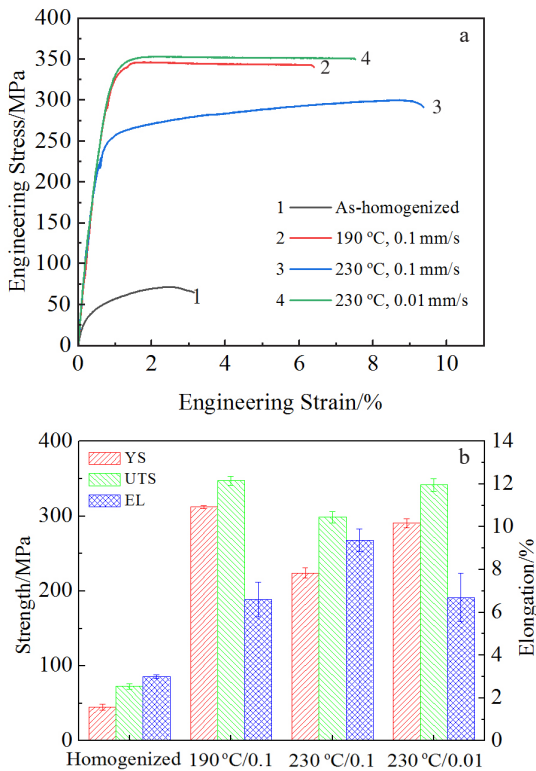


Fig.8 Engineering strain-stress curves (a) and YS, UTS and EL (b) of SiC_p/Mg-3.6Zn-0.6Y-0.2Ca composites extruded under different parameters

before and after extrusion. The yield strength (YS), ultimate tensile strength (UTS) and elongation (EL) are significantly improved after extrusion, as summarized in Fig. 8b. The YS, UTS and EL of the composite extruded at 0.1 mm/s at 190 °C are 312.0 MPa, 347.3 MPa and 6.6%, respectively. With increasing the extrusion temperature to 230 °C at 0.1 mm/s, the YS and UTS decrease while the elongation increases to 9.4%. As the extrusion speed decreases to 0.01 mm/s, the YS and UTS increase while the elongation decreases to 6.7%.

The strengthening mechanisms of the present composite include grain boundary strengthening, dislocation strengthening, solid solution, precipitate strengthening, thermal expansion strengthening and load transfer strengthening. The solid solution strengthening for the as-extruded composite studied here is regarded as its intrinsic strength and is limited for the improved YS because solid solution strengthening barely changes before and after extrusion^[28]. Load transfer strengthening (σ_{LT}) represents the interfacial bonding effect between the SiC particles and the matrix. Further, the interfacial bonding effect between the SiC_p and the matrix can be expressed as^[29]:

$$\sigma_{LT}=0.5f\sigma_{Mg} \quad (4)$$

where σ_{Mg} is the experimental value of 0.2% YS of the matrix (~77.3 MPa) and $f=2\%$ is the volume fraction of SiC nanoparticles present in the composite. According to Eq.(4), the improvement of YS by the load transfer effect is 0.773 MPa, and it can be insignificant or negligible for these as-extruded composites. Accordingly, the yield strength of the as-extruded SiC_p/Mg-3.6Zn-0.6Y-0.2Ca composites can be described as:

$$\sigma_y=\sigma_{y,homogenized}+\Delta\sigma_{gb}+M(\Delta\tau_p+\Delta\tau_d)+\Delta\sigma_{CET} \quad (5)$$

where $\Delta\sigma_{gb}$, $\Delta\tau_p$, $\Delta\tau_d$ and $\Delta\sigma_{CET}$ represent the increments in YS contributed by grain refinement, precipitate strengthening, dislocation strengthening and thermal expansion effects, respectively. As shown in Fig.2 and Fig.5, the microstructure of as-extruded SiC_p/Mg-3.6Zn-0.6Y-0.2Ca composite is comprised of primary DRXed region and a little unDRXed region. As such, the yield strength (σ_y) can be also predicted by the following equation:

$$\sigma_y=\sigma_{y,homogenized}+f_{DRX}\Delta\sigma_{y,DRX}+f_{unDRX}\Delta\sigma_{y,unDRX} \quad (6)$$

where $\Delta\sigma_{y,DRX}$ and $\Delta\sigma_{y,unDRX}$ are the strengthening increments in YS resulting from the DRXed and unDRXed regions, respectively; f_{DRX} and f_{unDRX} are the DRX volume fraction and the remnant deformed region in the as-extruded composites, respectively. According to Eq.(6), the yield strength (σ_y) for the recrystallized regions and unDRXed regions can be described as:

$$\Delta\sigma_{y,DRX}=\Delta\sigma_{gb,DRX}+M(\Delta\tau_p+\Delta\tau_{d,DRX}) \quad (7)$$

$$\Delta\sigma_{y,unDRX}=\Delta\sigma_{gb,unDRX}+M(\Delta\tau_p+\Delta\tau_{d,unDRX}) \quad (8)$$

In general, there are fewer dislocations in the DRX regions while the texture density of the DRX regions is different from that of the unDRX regions, so Eq.(7) and Eq.(8) can be given as^[9]:

$$\Delta\sigma_{y,DRX}=\Delta\sigma_{gb,DRX}+M(\Delta\tau_p) \quad (9)$$

$$\Delta\sigma_{y,unDRX}=M(\Delta\tau_{d,unDRX}) \quad (10)$$

As mentioned above, the grain sizes of as-extruded nanocom-

posites are relatively finer compared to as-homogenized counterpart, which contributes to the strength improvement. The increment in YS due to the refined grain size can be described as^[30]:

$$\Delta\sigma_{gb}=kd^{1/2} \quad (11)$$

where k is the Hall-Petch coefficient (125.8 MPa· $\mu\text{m}^{1/2}$), and d is the average grain size.

The large volume fraction of fine precipitates can inhibit dislocation movement, leading to Orowan strengthening, which can be described as^[31]:

$$\Delta\tau_p = M \frac{Gb}{2\pi\sqrt{1-\gamma}} \left(\frac{0.779}{\sqrt{f}} - 0.785 \right) d_p \ln \frac{0.785d_p}{b} \quad (12)$$

where $\Delta\tau_p$, M , G , b , v , d_p and f are the increment of strength from precipitation strengthening, strengthening coefficient (the value is 1.25^[29]), shear modulus of Mg matrix, Burger vector, Poisson ratio, average diameter and volume fraction of dynamic precipitate, respectively.

Further, dislocation strengthening can be illustrated as^[32]:

$$\Delta\tau_d = \alpha Gb\sqrt{\rho} \quad (13)$$

where α is a constant (0.2), ρ represents dislocation density and its value is reported as $10^{14}\sim 10^{16} \text{ m}^{-2}$ for the metals after severe deformation^[33]. For the present SiC_p/Mg-3.6Zn-0.6Y-0.2Ca composite, the value of ρ in the unDRX region is estimated as $1\times 10^{16} \text{ m}^{-2}$ after extrusion.

The thermal expansion coefficients is different for the

magnesium matrix and SiC particles, which can also contribute to the YS increment and can be expressed as^[29]:

$$\Delta\sigma_{\text{CET}} = \sqrt{3} \beta Gb \sqrt{\frac{12\Delta T\Delta\alpha V_p}{bd_p}} \quad (14)$$

where β represents strengthening coefficient (1.25); $V_p=2\%$ represents the volume fraction of SiC_p; ΔT is difference between extrusion temperature and test temperature; $\Delta\alpha$ stands for the difference in thermal expansion coefficient of the magnesium matrix and SiC particles; G and b represent the shear modulus (16.6 GPa) and Burgers vector (0.32 nm), respectively; V_p is the volume fraction of added SiC_p.

Based on Eq. (4~14), the contributions of individual strengthening mechanism in terms of grain refinement strengthening ($\Delta\sigma_{gb}$), precipitate strengthening ($\Delta\tau_p$), dislocation strengthening ($\Delta\tau_d$) and thermal expansion effect ($\Delta\sigma_{\text{CET}}$) can be added up to obtain the values of the calculated (σ_y). For instance, the σ_y for the composite extruded at 190 °C at 0.1 mm/s is calculated as 296.9 MPa, which is close to the experimental results ($\sigma_{0.2}$), as shown in Fig. 8. The difference between σ_y and $\sigma_{0.2}$ mainly relates to the neglected strengthening generated by the smallest precipitates. In addition, among the four strengthening mechanisms for the above calculation, grain refinement strengthening plays the most important role in the YS improvement for the present composites, which is much greater than both the thermal expansion effect and precipitate strengthening.

Fig. 9 shows the tensile fracture morphologies of SiC_p/

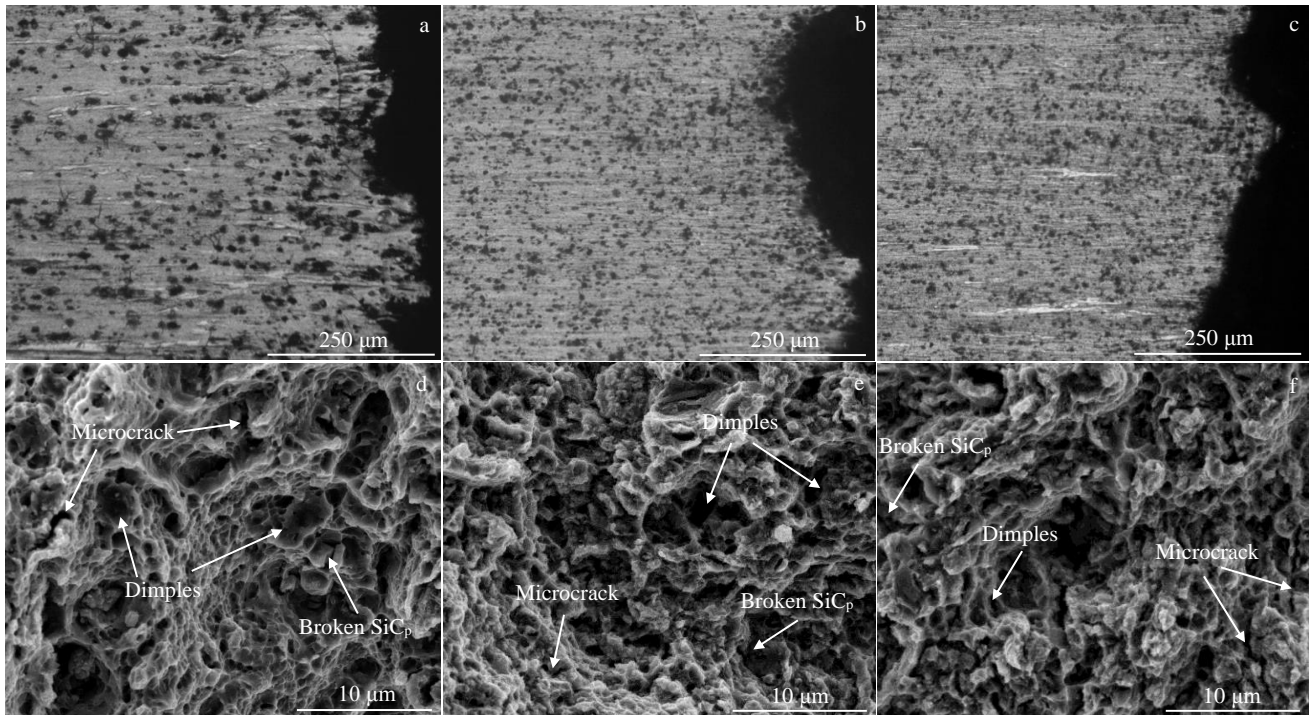


Fig.9 Tensile fracture morphologies of SiC_p/Mg-3.6Zn-0.6Y-0.2Ca composites extruded under different parameters: (a, d) 0.1 mm/s, 190 °C; (b, e) 0.1 mm/s, 230 °C; (c, f) 0.01 mm/s, 230 °C

Mg-3.6Zn-0.6Y-0.2Ca composites processed under different extrusion conditions. It can be seen that the DRX on the side of fracture tends to be complete under three extrusion conditions. Only a small amount of unDRX areas are found in the samples processed under $230\text{ }^{\circ}\text{C}/0.01\text{ mm}\cdot\text{s}^{-1}$ and $190\text{ }^{\circ}\text{C}/0.1\text{ mm}\cdot\text{s}^{-1}$, which is consistent with the above microstructure observation. Broken SiC_p can be observed from the front fractures in all the three samples. And the occurrence of microcracks is also found around the SiC_p . This can be attributed to the fact that the stress concentration in the vicinity of SiC_p is relatively large during the tensile test, resulting in a fracture of SiC_p and microcracking near SiC_p . In addition, by comparing the tensile frontal fractures, dimple size in the fracture for the sample processed under $230\text{ }^{\circ}\text{C}/0.1\text{ mm}\cdot\text{s}^{-1}$ is larger, which is consistent with variation trends of EL.

3 Conclusions

1) The grain sizes of the as-extruded composites significantly decrease as compared to the as-homogenized composite before extrusion. With increasing the extrusion speed or extrusion temperature, the size of recrystallized grains increases while the volume fraction slightly increases.

2) The sizes of dynamic precipitated phases increase with increasing the extrusion speed while the volume fractions decrease. The texture intensity under extrusion at 0.01 mm/s is significantly lower relative to that at 0.1 mm/s at the same extrusion temperature of $230\text{ }^{\circ}\text{C}$.

3) The YS, UTS and elongation of the composite extruded at $190\text{ }^{\circ}\text{C}$ at 0.1 mm/s are 312.0 MPa , 347.3 MPa and 6.6% , respectively. The grain refinement strengthening plays the most important role in the YS increment for the composites, which is much greater than the thermal expansion effect and precipitate strengthening.

References

- Wang X J, Xu D K, Wu R Z et al. *Journal of Materials Science and Technology*[J], 2018, 34: 245
- Peng Q, Sun Y, Ge B et al. *Acta Materialia*[J], 2019, 169: 36
- Pan F, Yang M, Chen X. *Journal of Materials Science & Technology*[J], 2016, 32(12): 1211
- You S, Huang Y, Kainer K U et al. *Journal of Magnesium and Alloys*[J], 2017, 5(3): 239
- Gao X, Nie J F. *Scripta Materialia*[J], 2007, 56(8): 645
- Imandoust A, Barrett C D, Al-Samman T et al. *Journal of Materials Science*[J], 2017, 52(1): 1
- Xu C, Zheng M Y, Xu S W et al. *Materials Science and Engineering A*[J], 2012, 547: 93
- Pan F, Mao J, Zhang G et al. *Progress in Natural Science Materials International*[J], 2016, 26(6): 630
- Du Y Z, Qiao X G, Zheng M Y et al. *Materials & Design*[J], 2015, 85: 549
- Hu K, Li C, Xu G et al. *Materials Science and Engineering A* [J], 2019, 742: 692
- Zhou M, Huang X, Morisada Y et al. *Materials Science and Engineering A*[J], 2020, 769: 138 474
- Kang X K, Nie K B, Deng K K et al. *Materials Characterization*[J], 2019, 151: 137
- Deng K K, Wang C J, Nie K B et al. *Acta Metallurgica Sinica (English Letters)*[J], 2019, 32(4): 413
- Jiang Q C, Wang H Y, Ma B X et al. *Journal of Alloys and Compounds*[J], 2005, 386(1-2): 177
- Guo Y C, Nie K B, Kang X K et al. *Journal of Alloys and Compounds*[J], 2019, 771: 847
- Hassan S F, Gupta M. *Materials Science and Engineering A*[J], 2005, 392(1-2): 163
- Wu K, Deng K, Nie K et al. *Materials & Design*[J], 2010, 31(8): 3929
- Wang X J, Hu X S, Wu K et al. *Materials Science and Engineering A*[J], 2015, 636: 138
- Zhao W, Huang S J, Wu Y J et al. *Metals*[J], 2017, 7(8): 293
- Li W, Deng K, Zhang X et al. *Journal of Alloys and Compounds*[J], 2017, 695: 2215
- Rohatgi P K, Asthana R, Das S. *International Metals Reviews* [J], 1986, 31(1): 115
- Saal J E, Wolverson C. *Acta Materialia*[J], 2014, 68: 325
- Ammouri A H, Kridli G, Ayoub G et al. *Journal of Materials Processing Technology*[J], 2015, 222: 301
- Tong L B, Zheng M Y, Cheng L R et al. *Materials Characterization*[J], 2015, 104: 66
- Li W, Deng K, Zhang X et al. *Materials Science and Engineering A*[J], 2016, 677: 367
- Wang L, Li X, Chao W et al. *Transactions of Nonferrous Metals Society of China*[J], 2016, 26(3): 704
- Stanford N. *Materials Science and Engineering A*[J], 2010, 527(10-11): 2669
- Nie K, Kang X, Deng K et al. *Journal of Materials Research* [J], 2018, 33(18): 2806
- Nie K, Deng K, Wang X et al. *Journal of Materials Research* [J], 2017, 32(13): 2609
- Hofstetter J, Rüedi S, Baumgartner I et al. *Acta Materialia*[J], 2015, 98: 423
- Khan F, Panigrahi S K. *Journal of Magnesium and Alloys*[J], 2015, 3(3): 210
- Du Y Z, Qiao X G, Zheng M Y et al. *Materials Science and Engineering A*[J], 2015, 620: 164
- Callister Jr W D, Rethwisch D G. *Fundamentals of Materials Science and Engineering: an Integrated Approach*[M]. New York: John Wiley & Sons, 2012

挤压参数对SiC颗粒增强Mg-3.6Zn-0.6Y-0.2Ca基复合材料组织和力学性能的影响

聂凯波^{1,2}, 杨安², 邓坤坤^{1,2}, 康心锴¹, 李亚楠¹

(1. 太原理工大学材料科学与工程学院, 山西太原 030024)

(2. 太原理工大学先进镁基材料山西省重点实验室, 山西太原 030024)

摘要: 研究了挤压前后SiC颗粒增强Mg-3.6Zn-0.6Y-0.2Ca基复合材料组织和力学性能。结果表明: 随挤压速率或挤压温度的增加, 再结晶晶粒的尺寸增加, 体积分数则略有增加。随挤压速率的增加, 动态析出相的尺寸增加, 体积分数减小。当挤压温度设定为230 °C时随挤压速率由0.01 mm/s增加到0.1 mm/s, 或当挤压速率设定为0.1 mm/s时挤压温度由190 °C增加到230 °C, 复合材料的屈服强度和抗拉强度降低, 而伸长率则逐渐增加。在优化的挤压参数(190 °C, 0.1 mm/s)下, 挤压态复合材料的屈服强度、抗拉强度和伸长率分别为312.0 MPa, 347.3 MPa和6.6%; 其中晶粒细化对强度提升的贡献高于热错配强化与析出强化。

关键词: SiC_p/Mg-Zn-Y-Ca复合材料; 热挤压; 微结构; 力学性能

作者简介: 聂凯波, 男, 1984年生, 博士, 教授, 太原理工大学材料科学与工程学院, 山西太原 030024, 电话: 0351-6010021, E-mail: niekaibo@tyut.edu.cn